Assessing Bjerknes Compensation for Climate Variability and Its Time-Scale Dependence

YINGYING ZHAO AND HAIJUN YANG

Laboratory for Climate and Ocean–Atmosphere Studies, Department of Atmospheric and Oceanic Sciences, School of Physics, Peking University, Beijing, China

ZHENGYU LIU

Department of Atmospheric and Oceanic Sciences, and Nelson Center for Climate Research, University of Wisconsin–Madison, Madison, Wisconsin, and Laboratory for Climate and Ocean–Atmosphere Studies, Department of Atmospheric and Oceanic Sciences, School of Physics, Peking University, Beijing, China

(Manuscript received 13 December 2015, in final form 27 April 2016)

ABSTRACT

The Bjerknes compensation (BJC) refers to the tendency for changes in the atmosphere heat transport (AHT) and ocean heat transport (OHT) to compensate each other. However, the nature of this compensation varies with the time scale of changes. In this study, a new approach was developed to diagnose BJC for climate variability by considering the correlation between AHT and OHT and their relative magnitudes. The correlation is equivalent to the cosine of phase difference between AHT and OHT. For high-frequency climate variability, AHT lags or leads OHT by $\pi/2$, the correlation is zero, and BJC does not occur concurrently. For low-frequency climate variability, AHT lags or leads OHT by π, the correlation is -1, and BJC is concurrent. With increasing time scale, the phase difference between AHT and OHT changes from $\pi/2$ to π, and the BJC reaches equilibrium. A coupled box model is used to justify the approach and to understand the temporal change of BJC from a theoretical perspective. The correlation and BJC rate derived from theory and from the box model exhibit similar transient behaviors, approaching equilibrium monotonically with increasing time scale. The equilibrium BJC is established at decadal time scale. Since the BJC is closely related to climate feedback, a proper identification of BJC processes in climate variability can reveal the nature of dominant climate feedback processes at different time scales.

1. Introduction

Meridional heat transports (MHTs) in the atmosphere and ocean are critical for maintaining energy balance of Earth's climate system. The MHTs vary on multiple time scales, and the variations of atmosphere heat transport (AHT) and ocean heat transport (OHT) are related to each other. Bjerknes (1964) first proposed the hypothesis that if the net radiation forcing at the top of the atmosphere (TOA) and the ocean heat storage do not vary too much, the total energy transport by the climate system would not vary too much either; in other words, any large variations in AHT and OHT should be equal in magnitude and opposite in sign. This simple scenario has become known as the Bjerknes compensation (BJC)—that is, a negative relationship between the change in AHT and the change in OHT.

The BJC has been confirmed to be valid in many studies, in models ranging from simple energy balance models (EBMs; e.g., Lindzen and Farrell 1977; Stone 1978; North 1984; Langen and Alexeev 2007; Rose and Ferreira 2013; Liu et al. 2016) to complex climate models (e.g., Clement and Seager 1999; Shaffrey and Sutton 2006; Cheng et al. 2007; Van Der Swaluw et al. 2007; Kang et al. 2008, 2009; Vellinga and Wu 2008; Donohoe et al. 2013; Farneti and Vallis 2013; Rose and Ferreira

Denotes Open Access content.

Corresponding author address: Haijun Yang, Department of Atmospheric and Oceanic Sciences, School of Physics, Peking University, 209 Chengfu Road, Beijing 100871, China.
E-mail: hjyang@pku.edu.cn

DOI: 10.1175/JCLI-D-15-0883.1

2013; Yang et al. 2013; Seo et al. 2014; Yang and Dai 2015). Usually, the BJC is valid on decadal and longer time scales based on coupled model studies (e.g., Shaffrey and Sutton 2006; Van Der Swaluw et al. 2007; Farneti and Vallis 2013). The BJC can occur in internal climate variability (e.g., Shaffrey and Sutton 2006) and in climate responses to external forcing (e.g., Vellinga and Wu 2008; Rose and Ferreira 2013; Yang and Dai 2015). It varies widely among models, at various time scales and at different latitudes, and is measured by the BJC rate, which is defined as the ratio of anomalous AHT to anomalous OHT.

The BJC rate is essentially determined by the overall climate feedback, which denotes the general relationship between the net TOA radiative flux and surface temperature. Our recent studies (Liu et al. 2016; Yang et al. 2016) developed a theory that links the BJC rate with local climate feedback explicitly. Specifically, AHT can perfectly compensate OHT in the absence of local climate feedback, undercompensate OHT if climate feedback is negative everywhere, or overcompensate OHT in the presence of positive local climate feedback. These theoretical studies provided explanations for different BJC behaviors in various previous modeling studies (e.g., Kang et al. 2008, 2009; Vellinga and Wu 2008; Enderton and Marshall 2009; Vallis and Farneti 2009; Zhang et al. 2010; Farneti and Vallis 2013; Yang et al. 2013; Seo et al. 2014).

The BJC theory developed in Liu et al. (2016) and Yang et al. (2016) applies only to equilibrium responses in a coupled system. There is no theory so far on the BJC for climate variability. Previous assessments on the BJC for climate variability were mostly based on coupled models and used somewhat arbitrary methods, which range from the correlation between AHT and OHT to the ratio of peak magnitudes of AHT and OHT changes (Van Der Swaluw et al. 2007). Such assessments cannot clearly distinguish different behaviors of the BJC: overcompensation, undercompensation, or perfect compensation. Moreover, many coupled models have demonstrated that the BJC is good for low-frequency variability, and the BJC rate was found to increase with increasing time scale (e.g., Shaffrey and Sutton 2006). These theories lead to several questions. How can we assess the BJC for climate variability reasonably? How does the BJC change with time scales? Is the BJC enhanced toward an equilibrium BJC as time scale increases? Is the BJC for low-frequency climate variability equivalent to an equilibrium BJC?

This work is an attempt to understand transient behaviors and time scales of BJC for climate variability from a theoretical perspective using the box model of Yang et al. (2016). First, we develop a comprehensive approach to diagnose BJC for climate variability and provide an example from a coupled climate model. Second, the coupled box model is used to exhibit transient change of BJC for climate variability by perturbing the model with constant, periodic, or stochastic freshwater forcing. The temporal changes of BJC in all three forcing situations are similar, approaching the equilibrium BJC rate monotonically with increasing time scale, and an equilibrium BJC is established at the decadal time scale and beyond. Third, a theoretical solution to transient BJC is obtained and then used to explain the numerical results in the box model. We will show that the BJC for climate variability is equivalent to the theoretical BJC. In this paper, we emphasize that the time-scale dependence of BJC is unique because it is not affected by the variations of AHT, OHT, or other climate variables, which can be monotonic, periodic, or even stochastically driven.

This paper is organized as follows. The approach to diagnose the BJC for climate variability is proposed in section 2. We introduce the coupled box model and equilibrium BJC rate briefly in section 3. Numerical results from the coupled box model under different forcing scenarios are shown in section 4. We provide theoretical explanations for the transient BJC based on the two-box-ocean coupled model in section 5. Summary and discussion are given in section 6.

2. BJC for climate variability

The low-frequency variations of AHT and OHT usually have a high negative correlation with each other, as illustrated by a long simulation using NCAR CESM1.0 (Fig. 1a; Yang et al. 2015). Similar results can be also found in previous works, such as Shaffrey and Sutton (2006) and Farneti and Vallis (2013). The variation in OHT is closely related to the fluctuation in the Atlantic meridional overturning circulation (AMOC; black curve in Fig. 1a), implying a critical role of thermohaline circulation (THC) in global energy balance (Farneti and Vallis 2013). Figure 1b shows clearly that both the correlation between AHT and OHT and the BJC rate increase monotonically with increasing time scale. Here, we want to emphasize that OHT and AHT in Fig. 1 are calculated directly from the velocity–potential temperature (VT) approach (Yang et al. 2015) instead of indirectly from the heat fluxes at the ocean surface and at the TOA. This assures the independency of AHT and OHT from each other. Different from the BJC definition in Van Der Swaluw et al. (2007), we propose a new formula to assess the BJC rate for general climate variability:

$$C_R \equiv r\frac{\sigma_{F_a}}{\sigma_{F_o}}, \tag{1}$$

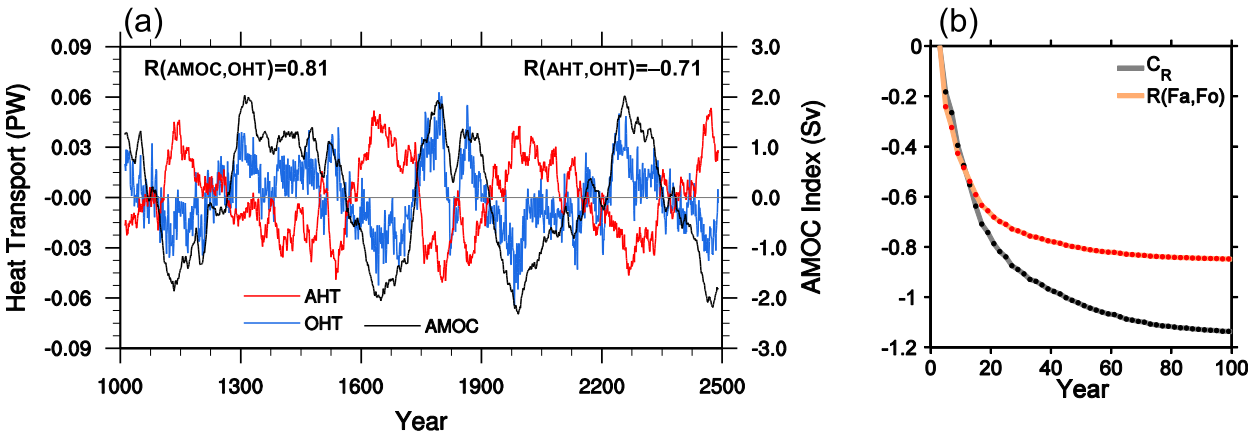

FIG. 1. (a) Time series of anomalous AHT (red; PW, 1 PW = 10^{15} W), OHT (blue; PW), and AMOC index (black; Sv) from a long simulation using NCAR CESM1.0. The AMOC index is defined as the maximum value of the streamfunction over 20°–70°N and between 300 and 2000 m in the Atlantic. The climatological mean values are removed first and then the anomalous data are filtered using the 21-yr running mean. AHT and OHT are calculated directly from the VT approach (Yang et al. 2015) and averaged over 30°S–70°N. The correlation between AMOC and OHT is 0.81 and that between OHT and AHT is −0.71, which are above the 99% significance level. (b) Changes of correlation between AHT and OHT (red) and of the BJC rate (black) with time scale. The x axis is time scale, where a number (e.g., N) means that the data are first filtered by N-yr running mean, and then the correlation and BJC are calculated using the filtered data.

where r is an instantaneous correlation coefficient between AHT and OHT, and σ_{F_a} and σ_{F_o} are standard deviations of AHT and OHT, respectively. The variable C_R is actually a regression coefficient that can be obtained by linearly regressing AHT with respect to OHT. This definition considers the differences in both phase and amplitude between AHT and OHT. It is a significant improvement from previous definitions and allows us to identify the BJC neatly and affirmatively. A negative correlation ($r < 0$) suggests a concurrent compensation between AHT and OHT, and the BJC rate is determined by both the correlation and the ratio of AHT and OHT standard deviations. If the correlation is low enough and below a certain significance level ($r \to 0$), there will be no statistically significant compensation. Positive correlation ($r \geq 0$) suggests no compensation. In sections 4 and 5, we will show that the correlation coefficient r is equivalent to the cosine of the phase difference between AHT and OHT, cosδ. When AHT and OHT move toward being out of phase, $\delta \to \pm 180°$ and cos$\delta \to -1$; as a result, the correlation $r \to -1$ and the BJC approaches its equilibrium value. In addition, the absolute value of BJC rate $|C_R|$ can be larger, equal to, or smaller than 1, corresponding to overcompensation, perfect compensation, or undercompensation (Yang et al. 2016), respectively, which are in turn determined by the overall local climate feedback. Therefore, the definition in Eq. (1) implies also the overall climate feedback situation for certain climate variability.

3. A coupled box model

The model consists of a two-box atmosphere and a four-box ocean (Fig. 2; see Yang et al. 2016 for more details). The atmosphere is assumed to mix the heat perfectly in the zonal direction and is always in quasi equilibrium with the surface ocean. The ocean model was based on Stommel (1961) and further developed in many studies (e.g., Marotzke 1990; Huang et al. 1992; Nakamura et al. 1994, hereinafter NSM94; Tziperman et al. 1994; Marotzke and Stone 1995, hereinafter MS95). The atmospheric boxes are placed between the equator and 75°N, and the ocean boxes represent the ocean in the Northern Hemisphere. Details about the model configuration can be found in Yang et al. (2016), and model parameters are listed in Table 1.

In the coupled box model, in response to a perturbation forcing of OHT, such as freshwater forcing, the equilibrium BJC rate is, as derived analytically in Yang et al. (2016), the following:

$$C_{\mathrm{R0}} \equiv \frac{\Delta F_a}{\Delta F_o} = -\frac{1}{1 + B/2\chi} < 0. \qquad (2)$$

Equation (2) states that C_{R0} is determined only by two climate parameters—the local climate feedback parameter B and the atmosphere heat transport coefficient χ—or by the nondimensional parameter b ($=B/\chi$). In a stable climate system, $B > 0$ usually representing an overall negative climate feedback; therefore, C_{R0} is

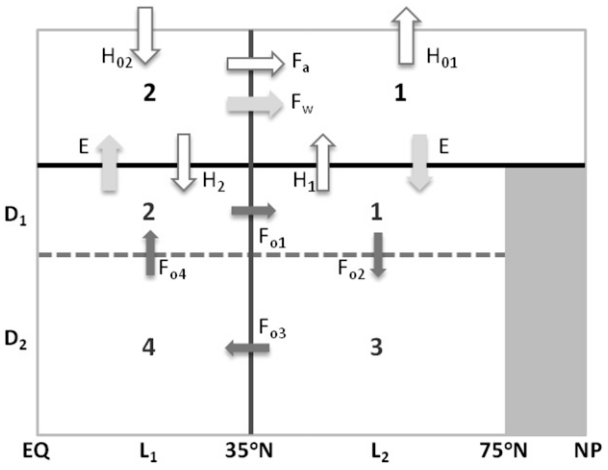

FIG. 2. Schematic plot of the coupled box model. Boxes 1 and 3 represent the upper and lower layers of the extratropical ocean, respectively, and boxes 2 and 4 of the tropical ocean, respectively. The variables D_1 and D_2 are the depths of upper- and lower-ocean layers, respectively. The variables L_1 and L_2 are the meridional scales of the tropical and extratropical boxes, respectively. The variables H_1 and H_2 are the ocean heat gains through the sea surface in the extratropics and tropics, respectively. The variables H_{01} and H_{02} are the net energy gains at the TOA in the extratropics and tropics, respectively. The variable E is the net freshwater loss in the tropics, or the net freshwater gain in the extratropics. The variable F_a is the meridional atmosphere energy transport. The variable F_w is the meridional atmosphere moisture transport. The variables F_{o1}–F_{o4} illustrate qualitatively the heat transports among different boxes.

always negative or the changes in AHT and OHT always compensate each other. Based on available observations, B has been estimated to be around 1.55–1.7 $\mathrm{W\,m^{-2}\,K^{-1}}$ (MS95; Kang et al. 2009; Rose and Ferreira 2013), whereas χ has a relatively wider range from 0.6 (North 1975) to 1.3 $\mathrm{W\,m^{-2}\,K^{-1}}$ (MS95), which is closely related to the parameterization of AHT. It is worth noting that Eqs. (1) and (2) are equivalent under constant forcing when the correlation coefficient $r = -1$ for out-of-phase changes in AHT and OHT, and σ_{F_a} and σ_{F_o} are equilibrium responses ΔF_a and ΔF_o.

The following variables will be used later on in discussion: $T_s = T_2 - T_1$, which is the SST contrast between the tropical box T_2 and extratropical box T_1; $S_s = S_2 - S_1$, which is the surface salinity contrast between the tropical box S_2 and extratropical box S_1; $q = \kappa(\alpha T_s - \beta S_s)$, which represents the ocean meridional mass transport or the THC, where κ is a constant parameter that sets the reference turnover time scale for a surface ocean box and α and β are the thermal and haline expansion coefficients of seawater, respectively; and F_o, F_a, and F_t, which represent OHT, AHT, and total MHT, respectively. More detailed descriptions for these variables can be found in Yang et al. (2016).

4. Transient changes in perturbation experiments

a. Constant freshwater perturbation

To understand the dynamics of BJC, a series of freshwater perturbation experiments were performed by imposing a sudden onset of a constant salinity tendency in the extratropical ocean box on Eq. (2a) of Yang et al. (2016):

$$h_{\mathrm{fw}} = h_0 = \text{constant}. \tag{3}$$

Under constant forcing, the BJC rate C_R approaches its analytical value C_{R0} monotonically, although the transient evolutions of AHT and OHT are not monotonic. Figure 3 shows the transient climate changes when 0.1-Sv ($1\ \mathrm{Sv} \equiv 10^6\,\mathrm{m^3\,s^{-1}}$) freshwater ($h_0 = 3.5 \times 10^{-10}\,\mathrm{psu\,s^{-1}}$) is removed from the extratropical ocean box. Here, both tropical and extratropical climate feedbacks are assumed to be negative ($B = 1.7\,\mathrm{W\,m^{-2}\,K^{-1}}$) so that the equilibrium BJC is determined from Eq. (2) as $C_{\mathrm{R0}} = -0.6$ (Fig. 3d). Changes in the box-model climate are obtained by removing the equilibrium state. Reducing freshwater in high latitudes results in the weakening of the meridional salinity gradient ($\Delta S_s < 0$; Fig. 3b), enhancing the THC ($\Delta q > 0$) and resulting in more poleward OHT ($\Delta F_o > 0$; Fig. 3c). This warms the extratropical ocean and results in the weakening of meridional temperature gradient ($\Delta T_s < 0$; Fig. 3b). As a result, AHT decreases ($\Delta F_a < 0$) and compensates partially for the increased OHT (Fig. 3c). Changes in the THC, S_s, and T_s as well as changes in AHT and OHT retreat slightly after they peak at around 200 years because of the feedbacks among them. However, the ratio of AHT and OHT approaches the analytical value monotonically (Fig. 3d).

Figure 3 shows that the time scale of quasi-equilibrium response in the box model is around 200 years. This time scale can be simply understood as the advective time scale of the THC (MS95), which is roughly estimated as $T_{\mathrm{eq}} = 2\pi/(\kappa\alpha T_s)$, where κ is the ocean advective time-scale coefficient and α is the water thermal expansion coefficient. Using the parameters in Table 1, $T_s = 27.4$°C and $T_{\mathrm{eq}} \approx 240$ yr. This is the quasi-equilibrium compensation time scale, as shown in Fig. 3d. The compensation is only slightly affected by the evolution of lower ocean, which has a much longer time scale (blue and green curves in Fig. 3a). This time scale can be also understood as the longest eigenperiod of the coupled box model (see discussion in section 5).

It is worth mentioning that the system's time scale is also intrinsically related to climate feedbacks (Roe 2009). In Yang et al. (2016), it is shown that the equilibrium time scale of the BJC varies from several

TABLE 1. Parameters used in this study.

Parameter	Physical description	Units	Value	Reference	Note
A_1	Net incoming radiation at box 1 and 2	$W\,m^{-2}$	−40	MS95	—
A_2			90		
B_1	Local climate feedback parameter in box 1 and box 2	$W\,m^{-2}\,K^{-1}$	1.7	MS95 NSM94	—
B_2			1.7		
$c\rho_0$	Heat capacity of a unit water volume	$J\,m^{-3}\,K^{-1}$	4×10^6	MS95	—
D_1	Depth of upper and lower boxes	m	400	—	—
D_2			4000		
G_{01}	Entire surface area north of the dividing latitude	m^2	1.25×10^{14}	MS95	—
L_1	Meridional scale of low- and high-latitude boxes	° lat	35°	MS95	—
L_2			40°		
S_0	Reference salinity	psu	35.0	MS95	—
α	Thermal expansion coefficient	K^{-1}	2.5×10^{-4}	—	—
β	Haline contraction coefficient	psu^{-1}	7.5×10^{-4}	—	—
ϵ	Ratio of ocean area of box 1 to G_{01} (i.e., G_1/G_{01}, $\epsilon \le 1$)	—	0.2	MS95	Atlantic sector
ϵ_w	Ratio of ocean and catchment area to G_{01}, $\epsilon \le \epsilon_w \le 1$	—	0.3	MS95	—
κ	Advective time-scale coefficient	s^{-1}	1.2×10^{-7}	—	$D = 5$ km
γ	Atmosphere moisture transport efficiency	$m\,s^{-1}\,K^{-1}$	1.2×10^{-10}	MS95	Factor of 1–3
χ	Atmosphere heat transport efficiency	$W\,m^{-2}\,K^{-1}$	1.3	MS95	—

decades to thousands of years as the climate feedback varies from strong negative (−1.7) to positive (0.5). Positive feedback can amplify the initial perturbation, and therefore it would take a longer time for the whole system to return to its equilibrium (Roe 2009). In this work, we focus on understanding the compensation time scale under given climate feedbacks. Specifically, why does the BJC approach the equilibrium state monotonically and on what time scale can the BJC be well established?

b. *Periodic freshwater perturbation*

A series of periodic perturbation experiments was designed to understand the time scale of BJC. These experiments were performed by removing freshwater in the extratropical box periodically, which were accomplished by adding a term of salinity tendency:

$$h_{\rm fw} = {\rm Re}(h_0 e^{i\omega t}), \tag{4}$$

where h_0 is the amplitude of the forcing (which is 3.5×10^{-10} psu s^{-1} for 0.1-Sv freshwater), and ω is the frequency of the forcing that ranges from zero to infinity. Figure 4 shows the model's responses to different forcing frequencies.

Both amplitude and phase of climate responses are related to the forcing frequency. The response amplitude is stronger for lower-frequency forcing (solid curves in Fig. 4). In a general climate system of long thermal inertia, the climate variability tends to exhibit a red noise response; that is, high-frequency forcing leaves insufficient time for the system to fully respond, resulting in the amplitudes of variables being smaller than those under low-frequency forcing. Under very-high-frequency forcing (e.g., a period of 5 yr), the model

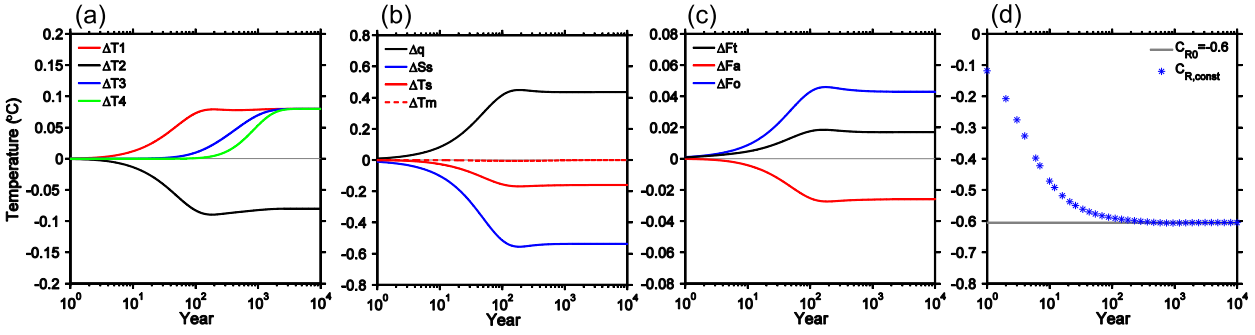

FIG. 3. Transient climate changes under constant freshwater forcing (−0.1 Sv) added in ocean box 1 (a) for ΔT (°C) in the four ocean boxes; (b) for Δq (Sv), ΔS_s (psu), ΔT_s (°C), and surface mean temperature ΔT_m (°C); (c) for heat transport changes (PW); and (d) for the BJC rate C_R from the box model (asterisks) and Eq. (2) (gray line). Here, the local climate feedback $B = 1.7\,W\,m^{-2}\,K^{-1}$.

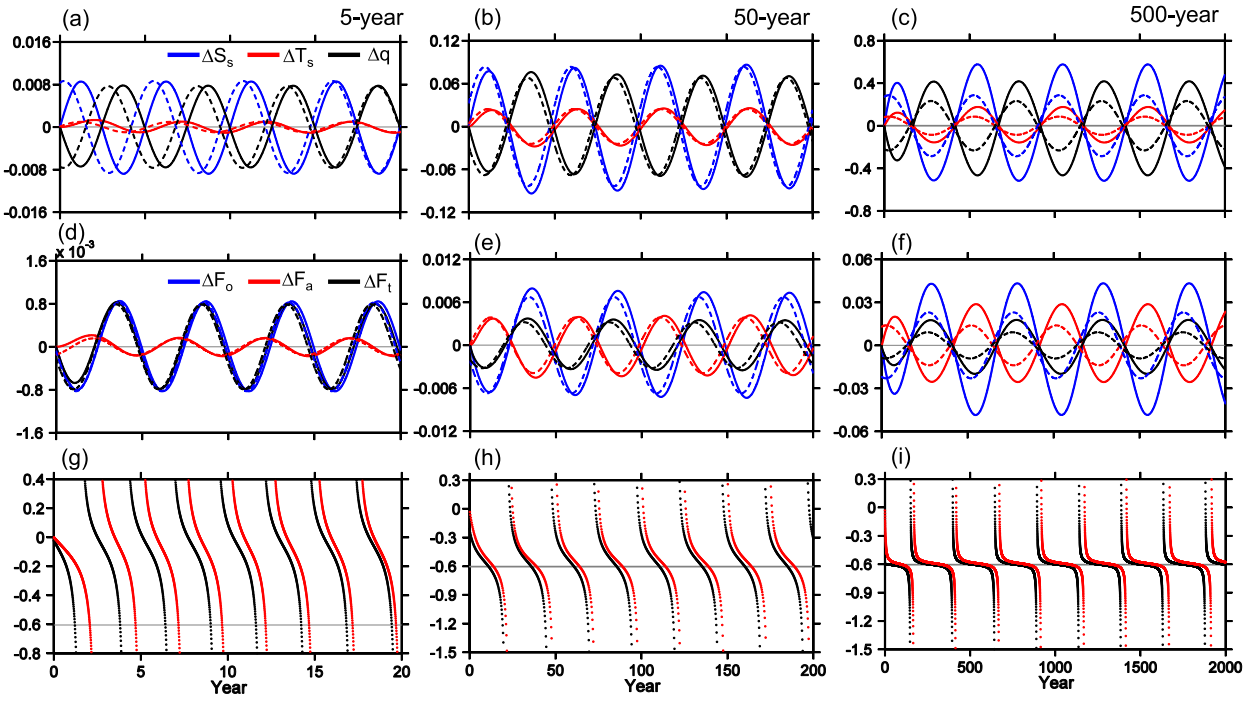

FIG. 4. Climate changes in different periodic freshwater forcing experiments: (left) 5-, (center) 50-, and (right) 500-yr period for (a)–(c) ΔT_s (°C; red), ΔS_s (psu; blue), and Δq (Sv; black); (d)–(f) heat transport changes (PW): AHT (ΔF_a; red), OHT (ΔF_o; blue), and THT (ΔF_t; black). The solid curves show numerical results from the coupled box model and the dashed curves for the theoretical results from the slab-ocean model. (g)–(i) the BJC rate C_R, which is simply calculated as $\Delta F_a/\Delta F_o$ from (d)–(f). The black and red dots are for numerical and theoretical results, respectively. Under low-frequency forcing, C_R concentrates around the theoretical value (−0.6) given by Eq. (2) as long as both ΔF_a and ΔF_o are nonzero.

temperature and salinity changes are so small (Fig. 4a) that they are negligible when compared to those under constant forcing (Fig. 3b), including the model heat transports also (Fig. 4d). The climate response is enhanced toward lower frequency (Figs. 4b,c,e,f), with the amplitude roughly unchanged for forcing frequency lower than 500 yr (figures not shown for frequency lower than 500 yr).

Changes of response amplitude under different forcing periods are clearly illustrated in Figs. 5a,b (circles). Each circle represents the peak response amplitude under a prescribed forcing frequency. We can see that the response amplitude becomes larger toward lower forcing frequency. Under high-frequency forcing (periods shorter than several decades), the response amplitude is negligible. When the forcing period (frequency) becomes longer (lower) than the advective time scale of the system (~250 yr), the response amplitude nearly reaches a constant, which is exactly the quasi-equilibrium response under constant forcing shown in Fig. 3. For a better comparison, the transient responses under constant forcing shown in Fig. 3 are also plotted in Figs. 5a,b (as solid curves). We can see that the patterns of amplitude change in response to different periodic forcing are similar to the transient climate changes under constant forcing, except that the periodic experiments need a longer time than the constant forcing experiment to reach the same magnitude. This is understood because the spinup from the sudden onset of constant forcing is dominated by fast time scales. When the forcing frequency is low enough, the amplitude merges with the equilibrium state of constant-forcing experiment.

The phase difference between temperature and salinity and that between OHT and AHT can be seen in Figs. 4a–f (solid curves). More visual changes in phase differences between the forcing and model variables are plotted in Fig. 5c. At the upper bound of forcing frequency (very high frequency), the peak response in S_s lags the forcing by about $\pi/2$ (or 90°, a quarter period) (dashed green). The peak response in T_s lags the forcing by about π (or 180°, a half period) (light red). Since AHT is determined by T_s, the phase difference between AHT and forcing is the same as that between T_s and forcing (dashed red). OHT is roughly determined by ocean mass transport, which is in turn roughly determined by S_s but with an opposite phase ($\Delta F_o \sim \Delta q \sim -\Delta S_s$). Therefore, both q and OHT lag the forcing by about $3\pi/2$ ($=2\pi - \pi/2$) (blue curves) and lag

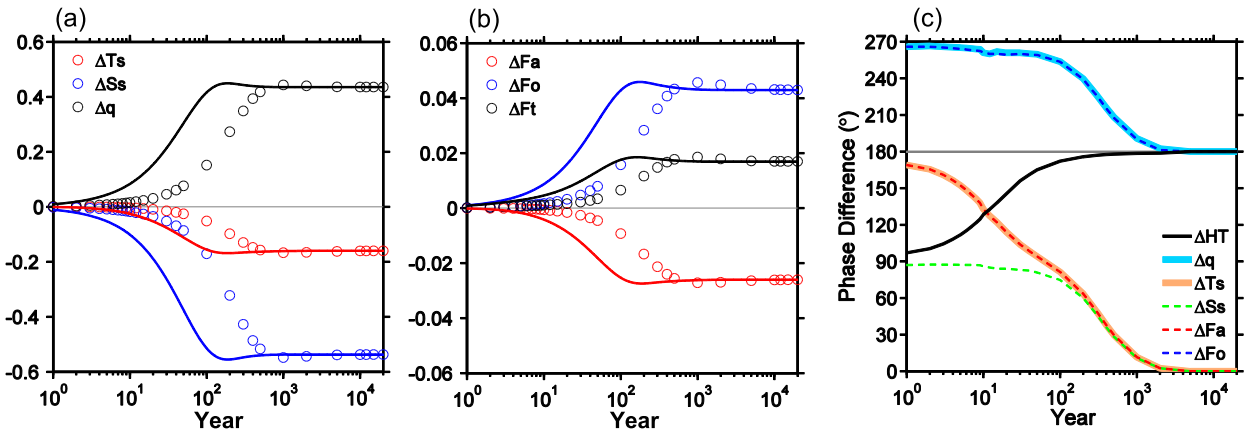

FIG. 5. Changes of climate response (magnitude) with different forcing periods: (a) Δq (Sv), ΔT_s (°C), and ΔS_s (psu) and (b) heat transport changes (PW). Circles are for periodic experiments. Curves shown in Figs. 3b,c are replotted here as solid curves for a better comparison. (c) Changes of phase differences with different forcing periods. Thick red (blue) curve shows phase difference between ΔT_s and external forcing (between Δq and external forcing); dashed green, red, and blue curves show phase differences between ΔS_s and external forcing, between ΔF_a and external forcing, and between ΔF_o and external forcing, respectively; black curve shows phase difference between ΔF_a and ΔF_o.

AHT by about $\pi/2$ (solid black curve). It is noticeable that the phase differences decrease monotonically with time scale. Toward the lower bound of forcing frequency, the phase difference between forcing and S_s (or T_s, F_a) becomes negligible. The most important feature is that OHT and AHT become out of phase (solid black curves in Fig. 5c); that is, they compensate each other.

The transient changes in correlation coefficient r between OHT and AHT and in the BJC rate C_R under the periodic forcing are plotted in Fig. 6. As mentioned in section 2, $r \sim \cos\delta$, which is exactly the case as shown in Fig. 6a. The values of r (blue asterisks) calculated from the time series of AHT and OHT (solid curves in Figs. 4d–f) are identical to those of $\cos\delta$ (black circles) based on the

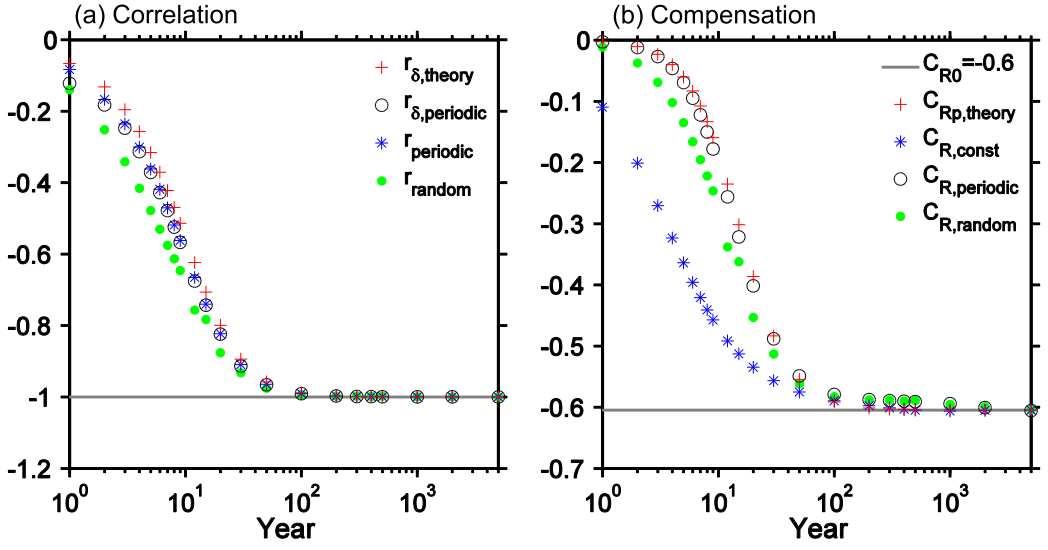

FIG. 6. (a) Changes of correlation between ΔF_a and ΔF_o with different forcing periods. Gray line shows $r = -1$. Red pluses are the theoretical values of r_δ (=cosδ) from Eq. (17), blue asterisks are for the correlation calculated directly from the time series of ΔF_a and ΔF_o shown in Figs. 4d–f, open circles are for the correlation calculated as the cosine of the phase difference shown as the black curve in Fig. 5c, and green dots are for the correlation from the stochastic forcing experiment. (b) As in (a), but for the BJC rate C_R. Gray line shows the theoretical value C_{R0} from Eq. (2). Red pluses are the theoretical values of C_{Rp} from Eq. (15); blue asterisks are for the constant freshwater forcing experiment (same as those in Fig. 3d); open circles for the periodic freshwater forcing experiment; and green dots for the stochastic forcing experiment. Open circles and green dots in (b) are calculated using Eq. (1).

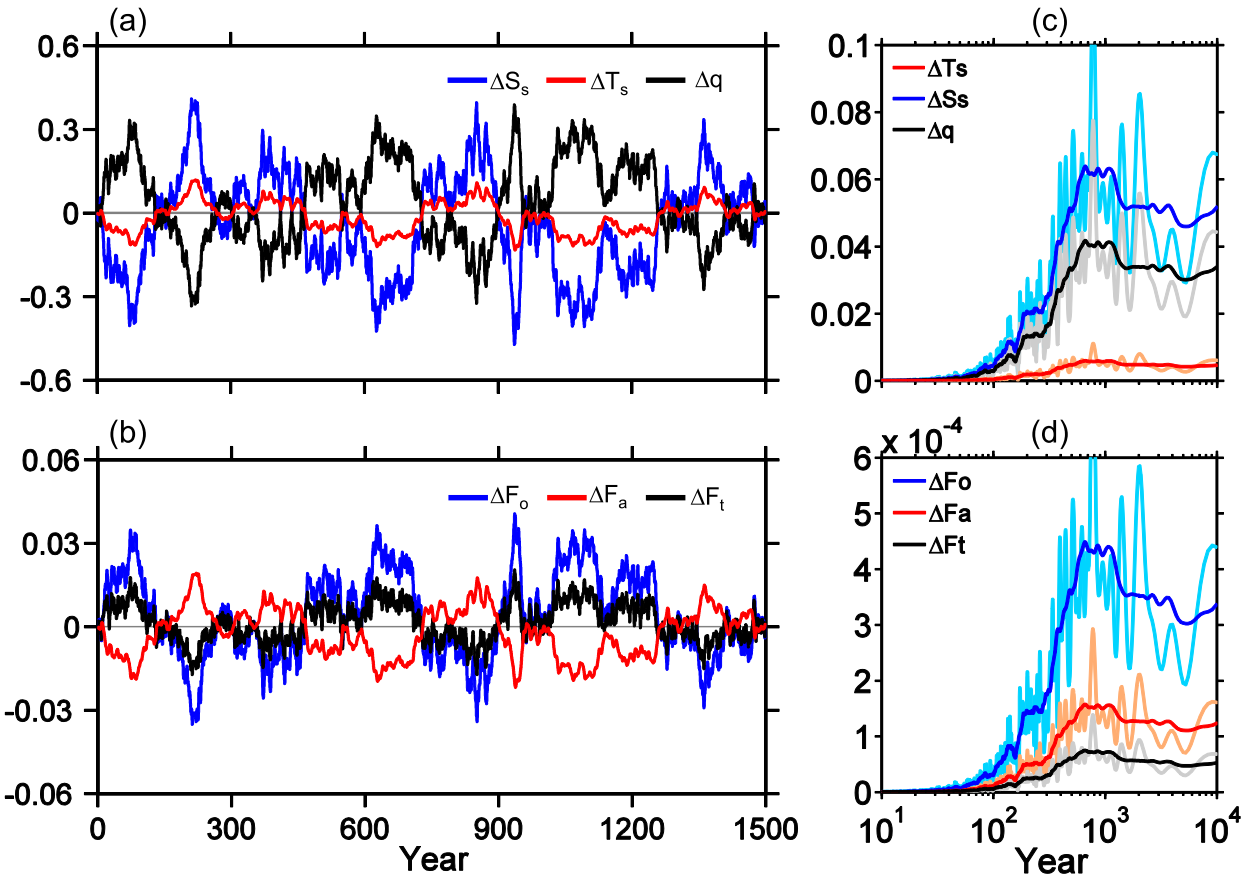

FIG. 7. Climate changes in the stochastic freshwater forcing experiment: (a) ΔT_s (°C; red), ΔS_s (psu; blue), and Δq (Sv; black) and (b) heat transport changes (PW) for ΔF_a (red), ΔF_o (blue), and ΔF_t (black). Power spectrums of these variables: (c) ΔT_s (red), ΔS_s (blue), and Δq (black) and (d) ΔF_a (red), ΔF_o (blue), and ΔF_t (black). In (c),(d), the darker color curves are the 99-point smoothed versions of the light color curves, respectively.

phase difference of AHT and OHT (solid black curve in Fig. 5c). Moreover, they are almost the same as the theoretical cosδ (red pluses) (given in section 5). As the forcing frequency decreases, AHT and OHT become out of phase, $\delta \rightarrow 180°$ and $r = \cos\delta \rightarrow -1$, and the BJC rate C_R for climate variability based on Eq. (1) (black circles in Fig. 6b), which exhibits a similar evolution to that under constant forcing (blue asterisks in Fig. 6b), approaches the equilibrium value C_{R0} (gray line in Fig. 6b) monotonically.

c. *Stochastic freshwater perturbation*

For a more general situation, an experiment with stochastic freshwater perturbation was performed by adding a term of white-noise salinity tendency:

$$h_{\mathrm{fw}} = h_0 \int_{\omega=0}^{\omega=\infty} e^{i\omega t}\, d\omega. \qquad (5)$$

The model responses to the random forcing are not random at all. There is distinct low-frequency variability in all variables (Fig. 7). Power spectral analysis reveals that the climate responses are enhanced toward lower frequency (Figs. 7c,d), similar to those shown in Fig. 4. There is a peak response to the random forcing with a time scale of 400–600 yr, which is particularly clear in ocean mass and heat transports. This time scale is consistent with the equilibrium response time scale illustrated in Figs. 5a,b and determined by the eigenmode of the four-box-ocean system (more discussion in section 5). However, the BJC rate C_R in this situation (green dots in Fig. 6b) still approaches the equilibrium BJC rate C_{R0} monotonically. The transient changes (green dots in Fig. 6) in both the correlation and the BJC rate show almost identical evolutions to those under periodic (black circles) forcing. In addition, despite its simplicity, the box-model simulations in Fig. 7 resemble the results from the coupled climate model in Fig. 1 very well.

5. A theory

To further understand time-scale dependence of the BJC, the four-box-ocean model is simplified in favor of

an analytical solution to the BJC under periodic forcing. The four-box ocean is reduced to a two-box (slab) ocean by assuming $T_1 = T_3 = T_4$ and $S_1 = S_3 = S_4$, similar to the slab ocean model used in MS95. The equations can be written in terms of T_s and S_s as follows:

$$\dot{T}_s = \frac{1}{\epsilon c \rho_0 D_1}[(A_2 - A_1 - BT_s) - 2\chi T_s] - 2qT_s \tag{6}$$

and

$$\dot{S}_s = \frac{2S_0}{\epsilon_w D_1}\gamma T_s - 2qS_s + h_{\text{fw}}. \tag{7}$$

Here, A_1 (<0) and A_2 (>0) are the net incoming radiation (W m^{-2}) at high and low latitudes, respectively; γ is the efficiency of atmosphere moisture transport; D_1 is the upper-ocean depth; c is seawater specific heat capacity; ρ_0 is seawater density; and S_0 is the reference salinity (35 psu). Time derivatives are denoted with dots over T_s and S_s. The variable ϵ indicates relative ocean coverage; ϵ_w is similar to ϵ but includes the influence of the catchment area of the ocean basin. All parameters used in this study are listed in Table 1, which were discussed in detail previously (NSM94; MS95; Yang et al. 2016). In fact, the analytical solution to the BJC given in Eq. (2) is identical for the slab-ocean and four-box-ocean models.

Considering infinitesimal perturbations (prime) of $T = \overline{T} + T'$ and $S = \overline{S} + S'$, where the overbar denotes an equilibrium state, the linearized versions of Eqs. (6) and (7) can be written in the matrix form as follows:

$$\frac{\partial}{\partial t}\begin{pmatrix} T_s' \\ S_s' \end{pmatrix} = \mathbf{M}\begin{pmatrix} T_s' \\ S_s' \end{pmatrix} + \begin{pmatrix} 0 \\ h_0 e^{i\omega t} \end{pmatrix}, \quad \text{where}$$
$$\mathbf{M} = \begin{pmatrix} M_A & M_B \\ M_C & M_D \end{pmatrix}. \tag{8}$$

Here,

$$M_A = -(F + 2\overline{q} + 2\kappa\alpha\overline{T}_s), \quad M_B = 2\kappa\beta\overline{T}_s,$$
$$M_C = 2(E - \kappa\alpha\overline{S}_s), \quad \text{and} \quad M_D = 2(\kappa\beta\overline{S}_s - \overline{q}),$$

and

$$E = \frac{S_0}{\epsilon_w D_1}\gamma \quad \text{and} \quad F = \frac{B + 2\chi}{\epsilon c \rho_0 D_1}.$$

Equation (8) is a nonhomogeneous linear system with constant coefficients, and its general solution can be written as the sum of the general solution to the homogeneous linear system plus one particular solution in response to external forcing. The homogeneous linear system is given by the following:

$$\frac{\partial}{\partial t}\begin{pmatrix} T_s' \\ S_s' \end{pmatrix} = \mathbf{M}\begin{pmatrix} T_s' \\ S_s' \end{pmatrix}. \tag{9}$$

The eigenvalues (λ_1, λ_2) of Eq. (9) can thus be obtained by solving the matrix **M**:

$$\lambda^2 - (M_A + M_D)\lambda + M_A M_D - M_B M_C = 0. \tag{10}$$

Here, $\lambda_1 + \lambda_2 = M_A + M_D$ and $\lambda_1\lambda_2 = M_A M_D - M_B M_C$. Given the parameters in Table 1, the discriminant of Eq. (10) is positive, and the two eigenvalues are $\lambda_1 = -1.65 \times 10^{-8}\,\text{s}^{-1}$ and $\lambda_2 = -1.15 \times 10^{-9}\,\text{s}^{-1}$, corresponding to damping time scales of 2 and 28 yr, respectively. The variable D_1 is set to 400 m ($\lambda_1 = -8.4 \times 10^{-9}\,\text{s}^{-1}$ and $\lambda_2 = -1.2 \times 10^{-9}\,\text{s}^{-1}$, if $D_1 = 1000$ m). The negative eigenvalues suggest that the slab-ocean model system is always a damping system without oscillation behavior when the external forcing is absent. Thus, any periodic behavior of the system has to come from external forcing. To understand Figs. 3–6, one only needs to obtain the particular solution to the nonhomogeneous system. Moreover, for the variability with time scales longer than 30 yr, the solution to the nonhomogeneous system will be determined solely by the particular solution, which can be written as follows:

$$T_s' = T_0 e^{i(\omega t - \theta)} \quad \text{and} \quad S_s' = S_0 e^{i(\omega t - \theta - \varphi)}, \tag{11}$$

where T_0 and S_0 are amplitudes of T_s' and S_s', respectively, θ is the phase difference of T_s' with respect to the external forcing, and φ is the phase difference between T_s' and S_s'. Here,

$$T_0 = \frac{M_B h_0}{\sqrt{M}} \quad \text{and} \quad S_0 = \frac{\sqrt{\omega^2 + M_A^2}h_0}{\sqrt{M}};$$
$$\cos\theta = \frac{-Q}{\sqrt{M}} \quad \text{and} \quad \cos\varphi = \frac{-M_A}{\sqrt{\omega^2 + M_A^2}}; \quad \text{and}$$
$$P = \omega(\lambda_1 + \lambda_2), \quad Q = \omega^2 - \lambda_1\lambda_2, \quad \text{and}$$
$$M = P^2 + Q^2.$$

The perturbations of the THC, AHT, and OHT are determined by T_s' and S_s'. They can be formulated as follows, according to Yang et al. (2016):

$$q' = \kappa(\alpha T_s' - \beta S_s'), \tag{12}$$
$$F_a' = \chi G_{01} T_s', \quad \text{and} \tag{13}$$
$$F_o' = c\rho_0 \epsilon G_{01} D_1(\overline{T}_s q' + \overline{q} T_s'). \tag{14}$$

The BJC rate can then be obtained:

$$C_{\text{Rp}} \equiv \frac{F_a'}{F_o'} = \text{Re}(C_{\text{R0}} e^{i\delta}) = r_\delta C_{\text{R0}}, \tag{15}$$

where

$$C_{R0} = \frac{2\chi}{\epsilon c \rho_0 D_1 \sqrt{\omega^2 + F^2}} \quad \text{and} \tag{16}$$

$$r_\delta \equiv \cos\delta = -\frac{F}{\sqrt{\omega^2 + F^2}}. \tag{17}$$

The variable C_{R0} is the ratio of amplitudes of F'_a and F'_o and therefore represents the magnitude of potential compensation, δ is the phase difference between OHT and AHT and reflects the extent of concurrent compensation, and r_δ is the correlation coefficient defined by $\cos\delta$.

Equation (15) clearly shows that the BJC rate is influenced by both amplitude and phase differences. Whether the forcing frequency matters to the BJC rate depends on the relative magnitudes of ω and F. Here, $F^{-1} = (\epsilon c \rho_0 D_1)/(B + 2\chi)$ can be understood as the equilibrium time scale for which the upper-ocean temperature fully responds to the local climate feedback B and atmosphere heat transport χ based on Eq. (6). Using parameters listed in Table 1, $F^{-1} \sim 3$ yr. Therefore, at the decadal time scale and beyond ($\omega \ll F; \omega^{-1} > 10$ yr), both the ratio of amplitude C_{R0} and the correlation coefficient r_δ are approaching constant. Thus, the BJC will reach the equilibrium quickly. Since at the short time scales, small r_δ (low correlation) weakens the BJC, to explore the BJC in a real climate system, one must smooth the data with a low-pass filter to reduce the influence of phase difference, as done in Fig. 1.

In fact, at the upper bound of forcing frequency ($\omega \to \infty$), $\cos\delta = 0$, AHT lags or leads OHT by $\pi/2$ (solid black curve in Fig. 5c), and there is no correlation between the two ($r_\delta = 0$). Also, $C_{Rp} = C_{R0} = 0$, and the system has almost no response to the external forcing, so there is no so-called BJC (dashed curves in Figs. 4a,d). With decreasing forcing frequency, the BJC rate increases monotonically as indicated by Eq. (15). At the lower bound of forcing frequency ($\omega \to 0$), $r_\delta = \cos\delta = -1$, AHT lags or leads OHT by π, and they are out of phase (Fig. 5c); $C_{Rp} = -(1 + B/2\chi)^{-1}$, which is exactly the equilibrium BJC given in Eq. (2). The values for r_δ and C_{Rp} are also plotted in Fig. 6 (red pluses) for comparison. The BJC for climate variability defined in Eq. (1) is practically identical to the theoretical solution in Eq. (15). The BJC rates obtained from different approaches have similar transient behaviors over time. They all merge with the equilibrium BJC after about 200 years.

The particular solutions under the periodic forcing based on Eqs. (11)–(14) are plotted in Fig. 4 (dashed curves), together with the numerical solutions from the coupled box model (solid curves in Fig. 4). We can see that the particular solutions to the slab ocean model are in good agreement with the general solutions to the four-box-ocean coupled model. Under high-frequency forcing, the phase difference between the particular solution and the numerical solution (Figs. 4a,d) exists because of the effect of eigenmode, which is important for variability at time scales shorter than 30 yr. When lowering the forcing frequency (longer time scales), the eigenmode diminishes (Figs. 4b,e) and the phase difference becomes negligible (Figs. 4c,f). Of course, there are some differences in the magnitudes of these solutions. After all, one is for a slab ocean and the other one is for a four-box ocean.

6. Summary and discussion

This work is an attempt to understand time-scale dependence of the BJC for general climate variability from a theoretical perspective. A new approach was proposed to diagnose BJC for climate variability. This approach considers both the phase difference between AHT and OHT variability and their relative amplitudes. The coupled model with the four-box ocean of Yang et al. (2016) was used to exhibit transient BJC for climate variability, whose solutions are very similar in different forcing scenarios, approaching the equilibrium BJC rate monotonically with increasing time scale. The theoretical solution to transient BJC was also obtained from a slab-ocean coupled model. The theoretical results are almost identical to the numerical results from the coupled box model with a four-box ocean. We showed that the BJC for climate variability is equivalent to the theoretical transient BJC. In addition, we stressed that the BJC exhibits a unique time-scale dependence that decreases monotonically with time scale and that this time-scale dependence is not affected by the variations of AHT, OHT, or other climate variables.

The approach to determine the BJC proposed in this work is important for diagnosing the compensation behavior in a complex climate system. Equation (1) tells us both the correlation between AHT and OHT and that their relative amplitudes are critical to determine the BJC. The correlation is actually equivalent to the cosine of their phase difference. The approach can exhibit overcompensation ($|C_R| > 1$), undercompensation ($|C_R| < 1$), or perfect compensation ($|C_R| = 1$). These different situations suggest different climate feedbacks, as shown in Yang et al. (2016). There should be positive (zero) feedback somewhere for overcompensation (perfect compensation). The BJC implies an overall climate feedback situation. Therefore, calculating the BJC properly for climate variability is important to understand climate feedback processes at various latitudes and various time scales. In fact, an inappropriate diagnosis of BJC is misleading, as shown in the "bad" plots

of Figs. 4g–i, which can go to infinity; such diagnosis would prevent us from understanding the fundamentals of a climate system.

The box model of course has its limitations, which were discussed in detail in Yang et al. (2016). For example, it does not include any wind-driven dynamics, so the wind-driven heat transport is missing. The equilibrium BJC rate is independent of heat transports, but Rose and Ferreira (2013) indicated that this independence cannot capture the range of behaviors in complex models. The theoretical solution is only for a slab ocean. We only considered small perturbations in this study. In the real world, perturbations may be significant, like the one under global warming. Nevertheless, the simple coupled box model can help us understand the fundamental mechanisms of the BJC and clarify the definition of BJC for climate variability. Comprehensive studies on the BJC in a complex coupled climate model are under way.

Acknowledgments. This work is jointly supported by the National Natural Science Foundation of China (41376007, 41176002, 91337106, and 40976007) and the National Basic Research Program of China (2012CB955200). We thank Dr. D. X. Sun for useful discussion on the theoretical perspective.

REFERENCES

Bjerknes, J., 1964: Atlantic air-sea interaction. *Advances in Geophysics*, Vol. 10, Academic Press, 1–82.

Cheng, W., C. M. Bitz, and J. C. H. Chiang, 2007: Adjustment of the global climate to an abrupt slowdown of the Atlantic meridional overturning circulation. *Ocean Circulation: Mechanisms and Impacts*, *Geophys. Monogr.*, Vol. 173, Amer. Geophys. Union, 295–313.

Clement, A. C., and R. Seager, 1999: Climate and the tropical oceans. *J. Climate*, **12**, 3383–3401, doi:10.1175/1520-0442(1999)012<3383:CATTO>2.0.CO;2.

Donohoe, A., J. Marshall, D. Ferreira, and D. McGee, 2013: The relationship between ITCZ location and cross-equatorial atmospheric heat transport: From the seasonal cycle to the Last Glacial Maximum. *J. Climate*, **26**, 3597–3618, doi:10.1175/JCLI-D-12-00467.1.

Enderton, D., and J. Marshall, 2009: Explorations of atmosphere–ocean–ice climates on an aquaplanet and their meridional energy transports. *J. Atmos. Sci.*, **66**, 1593–1611, doi:10.1175/2008JAS2680.1.

Farneti, R., and G. Vallis, 2013: Meridional energy transport in the coupled atmosphere–ocean system: Compensation and partitioning. *J. Climate*, **26**, 7151–7166, doi:10.1175/JCLI-D-12-00133.1.

Huang, R. X., J. R. Luyten, and H. M. Stommel, 1992: Multiple equilibrium states in combined thermal and saline circulation. *J. Phys. Oceanogr.*, **22**, 231–246, doi:10.1175/1520-0485(1992)022<0231:MESICT>2.0.CO;2.

Kang, S. M., I. M. Held, D. M. W. Frierson, and M. Zhao, 2008: The response of the ITCZ to extratropical thermal forcing: Idealized slab-ocean experiments with a GCM. *J. Climate*, **21**, 3521–3532, doi:10.1175/2007JCLI2146.1.

——, D. M. W. Frierson, and I. M. Held, 2009: The tropical response to extratropical thermal forcing in an idealized GCM: The importance of radiative feedbacks and convective parameterization. *J. Atmos. Sci.*, **66**, 2812–2827, doi:10.1175/2009JAS2924.1.

Langen, P. L., and V. A. Alexeev, 2007: Polar amplification as a preferred response in an idealized aquaplanet GCM. *Climate Dyn.*, **29**, 305–317, doi:10.1007/s00382-006-0221-x.

Lindzen, R. S., and B. Farrell, 1977: Some realistic modifications of simple climate models. *J. Atmos. Sci.*, **34**, 1487–1501, doi:10.1175/1520-0469(1977)034<1487:SRMOSC>2.0.CO;2.

Liu, Z., H. Yang, C. He, and Y. Zhao, 2016: A theory for Bjerknes compensation: The role of climate feedback. *J. Climate*, **29**, 191–208, doi:10.1175/JCLI-D-15-0227.1.

Marotzke, J., 1990: Instabilities and multiple equilibria of the thermohaline circulation. Ph.D. thesis, University of Kiel, 126 pp., doi:10.3289/ifm_ber_194.

——, and P. Stone, 1995: Atmospheric transports, the thermohaline circulation, and flux adjustments in a simple coupled model. *J. Phys. Oceanogr.*, **25**, 1350–1364, doi:10.1175/1520-0485(1995)025<1350:ATTTCA>2.0.CO;2.

Nakamura, M., P. H. Stone, and J. Marotzke, 1994: Destabilization of the thermohaline circulation by atmospheric eddy transports. *J. Climate*, **7**, 1870–1882, doi:10.1175/1520-0442(1994)007<1870:DOTTCB>2.0.CO;2.

North, G. R., 1975: Theory of energy-balance climate models. *J. Atmos. Sci.*, **32**, 2033–2043, doi:10.1175/1520-0469(1975)032<2033:TOEBCM>2.0.CO;2.

——, 1984: The small ice cap instability in diffusive climate models. *J. Atmos. Sci.*, **41**, 3390–3395, doi:10.1175/1520-0469(1984)041<3390:TSICII>2.0.CO;2.

Roe, G., 2009: Feedbacks, timescales, and seeing red. *Annu. Rev. Earth Planet. Sci.*, **37**, 93–115, doi:10.1146/annurev.earth.061008.134734.

Rose, B. E., and D. Ferreira, 2013: Ocean heat transport and water vapor greenhouse in a warm equable climate: A new look at the low gradient paradox. *J. Climate*, **26**, 2117–2136, doi:10.1175/JCLI-D-11-00547.1.

Seo, J., S. M. Kang, and D. M. Frierson, 2014: Sensitivity of intertropical convergence zone movement to the latitudinal position of thermal forcing. *J. Climate*, **27**, 3035–3042, doi:10.1175/JCLI-D-13-00691.1.

Shaffrey, L., and R. Sutton, 2006: Bjerknes compensation and the decadal variability of the energy transports in a coupled climate model. *J. Climate*, **19**, 1167–1181, doi:10.1175/JCLI3652.1.

Stommel, H., 1961: Thermohaline convection with two stable regimes of flow. *Tellus*, **13A**, 224–230, doi:10.1111/j.2153-3490.1961.tb00079.x.

Stone, P. H., 1978: Constraints on dynamical transports of energy on a spherical planet. *Dyn. Atmos. Oceans*, **2**, 123–139, doi:10.1016/0377-0265(78)90006-4.

Tziperman, E., J. R. Toggweiler, Y. Feliks, and K. Bryan, 1994: Instability of the thermohaline circulation with respect to mixed boundary conditions: Is it really a problem for realistic models? *J. Phys. Oceanogr.*, **24**, 217–232, doi:10.1175/1520-0485(1994)024<0217:IOTTCW>2.0.CO;2.

Vallis, G. K., and R. Farneti, 2009: Meridional energy transport in the coupled atmosphere–ocean system: Scaling and numerical experiments. *Quart. J. Roy. Meteor. Soc.*, **135**, 1643–1660, doi:10.1002/qj.498.

Van Der Swaluw, E., S. S. Drijfhout, and W. Hazeleger, 2007: Bjerknes compensation at high northern latitudes: The ocean

forcing the atmosphere. *J. Climate*, **20**, 6023–6032, doi:10.1175/2007JCLI1562.1.

Vellinga, M., and P. Wu, 2008: Relations between northward ocean and atmosphere energy transports in a coupled climate model. *J. Climate*, **21**, 561–575, doi:10.1175/2007JCLI1754.1.

Yang, H., and H. Dai, 2015: Effect of wind forcing on the meridional heat transport in a coupled climate model: Equilibrium response. *Climate Dyn.*, **45**, 1451–1470, doi:10.1007/s00382-014-2393-0.

——, Y. Wang, and Z. Liu, 2013: A modelling study of the Bjerknes compensation in the meridional heat transport in a freshening ocean. *Tellus*, **65A**, 60–73, doi:10.3402/tellusa.v65i0.18480.

——, Q. Li, K. Wang, Y. Sun, and D. Sun, 2015: Decomposing the meridional heat transport in the climate system. *Climate Dyn.*, **44**, 2751–2768, doi:10.1007/s00382-014-2380-5.

——, Y. Zhao, and Z. Liu, 2016: Understanding Bjerknes compensation in atmosphere and ocean heat transports using a coupled box model. *J. Climate*, **29**, 2145–2160, doi:10.1175/JCLI-D-15-0281.1.

Zhang, R., S. M. Kang, and I. M. Held, 2010: Sensitivity of climate change induced by the weakening of the Atlantic meridional overturning circulation to cloud feedback. *J. Climate*, **23**, 378–389, doi:10.1175/2009JCLI3118.1.